Transactions of Materials Research 1 (2025) 100008

Contents lists available at ScienceDirect

Transactions of Materials Research

journal homepage: www.sciencedirect.com/journal/transactions-of-materials-research

Elucidating the mechanism of strain-driven <100> dislocation loop formation in bcc iron

Hong-Bo Zhou [a,b], Xin-Ya Tang [a,b], Yu-Hao Li [a,b], Tian-Ren Yang [a,b], Hao-Xuan Huang [a,b], Qing-Yuan Ren [c], Guang-Hong Lu [a,b,*]

[a] Department of Physics, Beihang University, Beijing, 100191, China
[b] Beijing Key Laboratory of Advanced Nuclear Materials and Physics, Beihang University, Beijing, 100191, China
[c] Department of Mathematics and Physics, North China Electric Power University, Baoding, 071003, China

ARTICLE INFO

Keywords:
<100> Dislocation loop
Bcc iron and iron alloys
Anisotropic strain
Bi-loop reactions
Molecular dynamics

ABSTRACT

Dislocation loop is a primary indicator of irradiation, and has a profound impact on the microstructural evolution and thermo-mechanical properties of materials. Although both 1/2<111> and <100> loops are clearly identified in bcc metals after irradiation, the underlying mechanism of <100> loop formation remains elusive especially considering its low stability. Here, we explicitly demonstrate the formation of <100> loops through the interaction of two gliding 1/2<111> loops under uniaxial strain via molecular dynamics simulations, while there is no occurrence of <100> loops under strain-free conditions. Such strain-enhanced formation of <100> loops is different from conventional dislocation reaction mechanisms, which contain rigorous prerequisite conditions on the topology and size of the reactant loops, and thus provide a potential explanation for the frequent occurrence of <100> loops. The microscopic analysis suggests that the generation of <100> dislocation loops via bi-loop reaction is a complicated atomistic process involving the coordinated movement and/or rearrangement of multiple interstitials. The activation energy barriers of each reaction step are determined, and generally decrease with increasing uniaxial strain. Specifically, we develop a predictive model to describe the formation probability of <100> loops under different conditions, which is in good agreement with molecular dynamics simulations. These results shed new light on understanding the <100> loop formation, provide a direct link between simulations and experiments, and enable the accurate assessment of irradiation damage evolution in bcc metals.

1. Introduction

Irradiation of high-energy particles dramatically affects the microstructural evolution and properties of materials, and has been recognized and investigated for over 80 years [1]. Such effects, either detrimental under operational conditions (e.g., neutron damage for structural materials in nuclear system) or beneficial during manufacturing procedures (e.g., ion beam processing of semiconductor for the microelectronic industry) [2–4], should be governed by the generation, migration, recombination and accumulation of displacement defects, while these microscopic processes are not entirely understood. Because of the high formation energy (>4 eV) and distinct stress field, self-interstitial atoms (SIAs) are the typical displacement defects and are commonly considered as the primary indicators of particle irradiation [5]. The agglomerations of these interstitial atoms on a habit plane will induce the formation of dislocation loop, which is a major factor controlling the microstructure and thermo-mechanical response of materials under irradiation [6–9]. Based on the magnitude and direction of atomic transition, the dislocation loops are generally characterized by the Burgers vector. Intriguingly, two types of dislocation loops (i.e., 1/2<111> and <100> Burgers vectors) are explicitly identified in bcc metals using transmission electron microscopy [6,10–17]. This is, however, somehow different from the theoretical calculations [18,19], in which the formation energy of 1/2<111> loop is much lower than that of <100> loop, indicating the low possibility of <100> loop formation. Since the mobility of 1/2<111> loop is much higher than that with <100> Burgers vector and can be easily trapped by intrinsic defects, the presence of <100> loops may dramatically alter the performance of materials and induce the different response of bcc metals on irradiation [20]. Therefore, understanding the mysterious mechanism of <100> dislocation loops is a long-standing and essential topic of both scientific and technological importance, relevant to predicting the consequences of irradiation and

* Corresponding author. Department of Physics, Beihang University, Beijing, 100191, China.
E-mail address: lgh@buaa.edu.cn (G.-H. Lu).

https://doi.org/10.1016/j.tramat.2025.100008
Received 22 March 2025; Received in revised form 3 April 2025; Accepted 3 April 2025
Available online 3 April 2025

designing radiation-resistant materials.

Despite enormous research efforts in the past half century, there is no consensus on <100> loop formation in bcc metals and several potential mechanisms have been proposed. The first one was already reported in 1965 by Eyre and Bullough [21], who argued that a <110> shear of a faulted 1/2<110> loop can produce a <100> loop. However, because of the high energy cost for the stacking fault, the formation of a faulted loop in bcc metals is energetically implausible. Alternatively, Dudarev et al. claimed that the temperature dependence of the anisotropic elastic free energy has a profound effect on the relative stability of the 1/2<111> and <100> dislocation loops; the latter becomes more energetically stable at high temperatures (>823 K) [22]. This is consistent with experimental observations [23–25] and provides a thermodynamic interpretation for <100> loops in bcc iron (Fe), but lacks the kinetic mechanism in detail. Besides, atomistic simulations explicitly demonstrated that <100> loops can be transformed from 1/2<111> loops or C15 interstitial clusters directly, especially at high temperatures [19,26,27]. Nevertheless, these works mainly focused on the small SIA clusters. Since the activation energy for the transformation processes (considering the junction formation) is expected to increase with cluster size, the application of this mechanism to larger clusters remains very challenging. Moreover, molecular dynamics (MD) simulations suggested the formation of <100> loops in bcc metals during high-energy displacement cascades, which can be attributed to cascade overlap with pre-existing damages and/or the supersonic shockwave induced by cascade [28–30]. However, the probability of <100> loop formation largely depends on the incident energy and atomic mass, and should be extremely low in neutron irradiation cascades [30,31]. In addition, the dislocation reactions (i.e., interaction of two or three gliding 1/2<111> loops) have been considered a promising route for the formation of <100> loops. Although this mechanism is supported by some experiments [16,32] and MD simulations [5,18,33], there are some rigorous prerequisite conditions, including two equal-sized loops with an acute angle or coalescence of multiple loops simultaneously, leading to a rare event in reality. Making the matter even more complicated, extensive experiments suggested the decisive role of external stimuli (e.g. stresses [34–37], temperatures [13,23,38] and impurities [15,39,40]) in the formation of <100> loops in irradiated bcc metals, while the underlying physics of these effects remains to be elucidated.

Here, taking bcc Fe as an example, we explicitly demonstrated that anisotropic strain (both compression and tension) can obviously stimulate the formation of <100> loops via bi-loop reaction based on a series of comprehensive MD simulations. Different from the above-mentioned mechanisms, this process does not require any prerequisites (except for anisotropic strain) and reduces the limitations on the topology and size of the reactant loops, providing a potential explanation for the common occurrence of <100> loops. The distinct atomistic processes of interactions between two 1/2<111> loops are analyzed and the activation energies for each reaction step are obtained using both nudged elastic band (NEB) calculations and the Arrhenius formula. It is found that the anisotropic strain effectively reduces the activation energy of bi-loop reactions. Accordingly, we developed a predictive model to describe the probability of <100> loop formation in bcc Fe via bi-loop reactions, considering anisotropic strain and the difference in loop sizes. These results shed new light on understanding bi-loop reactions and <100> loop formation, and thus have broad implications to access the microstructural evolution and thermo-mechanical response of bcc metals under irradiation.

2. Computational methods

The molecular dynamics (MD) simulations were conducted using the extensively utilized Large-scale Atomic/Molecular Massively Parallel Simulator (LAMMPS) code [41]. The interactions between 1/2<111> dislocation loops were modeled under finite temperature and anisotropic strain conditions. The simulation box was oriented along x = [100], y = [010], and z = [001] axes, comprising 40 × 40 × 40 unit cells, with periodic boundary conditions (PBCs) in all directions (see Fig. 1). During the MD simulations, the lattice constant was adjusted in response to temperature variations to ensure an average system pressure of zero as the initial condition prior to applying strain. Two dislocation loops with intersecting glide prisms were created with Burgers vectors of 1/2[$\bar{1}\bar{1}$1] and 1/2[111], as shown in Fig. 1a [5,18,33,42]. The size of each reactant loop ranged from 37 to 91 SIAs. Uniaxial strains ranging from −3 % to 3 % were incrementally applied to each axis in 1 % steps, with the other two directions controlled using the isothermal-isobaric (NPT) ensemble to maintain zero pressure, as shown in Fig. 1b. The simulation system was then minimized using the conjugate gradient method and equilibrated in the canonical (NVT) ensemble. The temperature varied from 300 K to 1100 K, with the reaction time controlled within 1 ns and a timestep of 0.001 ps. For each condition, we repeated the simulations 10 times with different random initial velocities to mitigate random events and provide a rough estimate of the formation probability.

The NEB method is an effective approach for determining the minimum energy path (MEP), saddle point states, and migration energy barriers [43]. During the relaxation process of the bi-loop reaction, atomic configurations were extracted at 1 ps intervals and then minimized to serve as input configurations for the NEB calculation. In each NEB calculation, 20 images were utilized [33]. The final energy barrier was obtained by averaging the results of 5 cases. To fully assess the effective energy barrier for <100> loop formation, we also investigated the dependence of the time required for the formation of a pure <100> loop on temperature. The time was defined as the interval between the first contact of the two loops and the identification of a complete <100> loop using the Dislocation Extraction Algorithm (DXA) analysis [44].

We selected the embedded-atom-method (EAM) potential developed by Ackland et al. to model atomic interactions [45]. This potential was chosen because it qualitatively and quantitatively captures the properties of the single SIA and small SIA clusters, in close agreement with *ab initio* results [46]. Additionally, it accurately describes the relative stability of SIA clusters, showing that the 1/2<111> loop is more stable than the <100> loop [46]. Furthermore, other commonly employed iron-based potentials, namely A97 [47], M03 [48], and M07 [46], were used to verify the universality of obtained results. The simulation results were visualized with Open Visualization Tool (OVITO) [49], where SIAs were identified through the Wigner-Seitz method, and changes in dislocation Burgers vectors were analyzed using the dislocation extraction algorithm (DXA) [44].

3. Results and discussion

3.1. Interaction between two 1/2<111> dislocation loops in strain-free Fe

In order to investigate the influence of strain on the bi-loop reactions, the interaction of two gliding 1/2<111> dislocation loops in strain-free Fe should be determined firstly. As demonstrated previously [42,50], the interaction processes and final configurations are closely related to the size of reacting loops and temperatures. Therefore, a wide range of temperatures (~300–1100 K with an interval of 100 K) and loop size (~37–91 SIAs, the radius of 0.7–1.2 nm) are considered here. Generally, there are two distinct productions for the loop-loop interactions in strain-free Fe. The first one is the formation of a stable, immobile and three-dimensional complex (i.e., sessile complex), which consists of SIAs with different orientations. As shown in Fig. 2a, most of SIAs in the sessile complex maintain their initial orientations except for a junction line, while their habit plane rotates from {111} to {110}. The dumbbells in the junction region adopt the [001] direction via reaction of 1/2[111] + 1/2[1$\bar{1}\bar{1}$] = [001], which conserves the Burgers vectors and obeys the Kirchhoff's law. Because of the non-parallel structure and merged habit plane, the glide of this complex should be extremely difficult. Aside from the sessile complexes, a large cluster containing parallel SIAs along a

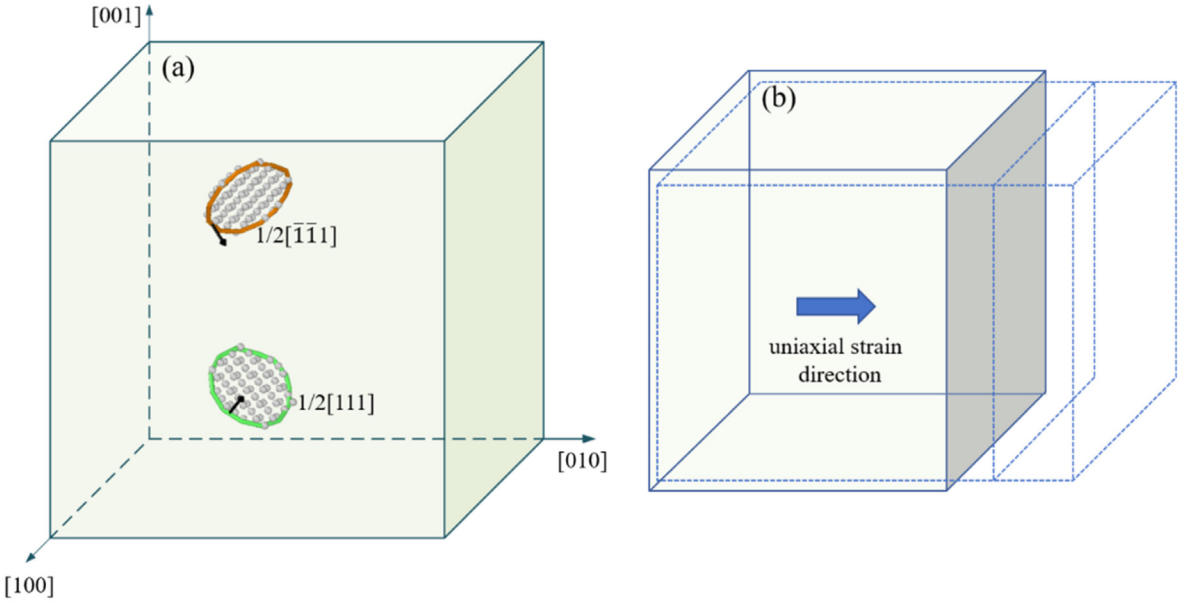

Fig. 1. Simulation model: (a) geometry of loop-loop interaction, (b) description of uniaxial strain applications. The periodic boundary conditions (PBCs) were applied in all directions.

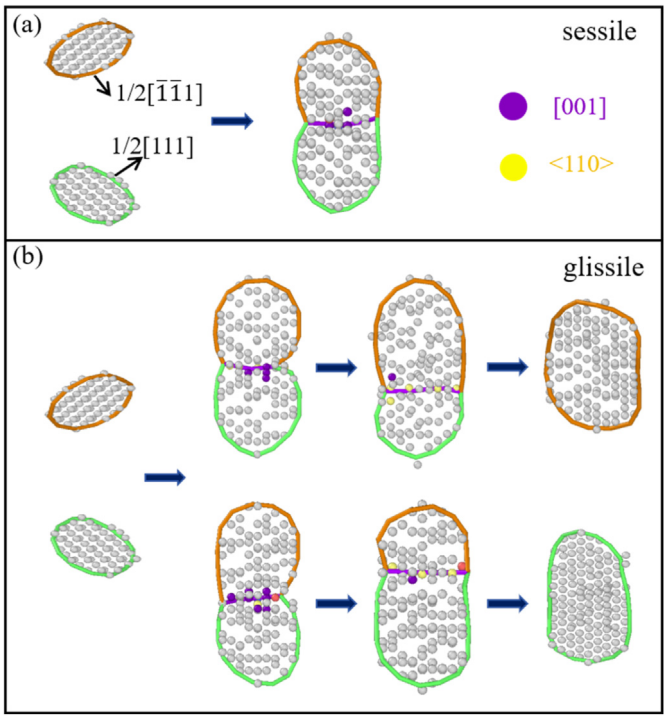

Fig. 2. Reaction process of the bi-loop reaction in strain-free Fe: (a) formation of a sessile complex, (b) formation of a glissile loop.

<111> direction (i.e., glissile loop) may also be formed by the coalescence of two dislocation loops in bcc Fe. In this case, one of the reacting loops changes the orientation of its SIAs to the other, as shown in Fig. 2b, which actually leads to the growth of dislocation loops.

It is important to note that the formation energy of the sessile complexes should be much higher than that of parallel dislocation loops along <111> direction [42], which provides a thermodynamic driving force for the structural transformation. Accordingly, as shown in previous studies [42,50] and in the present work, the transition of sessile complex to a perfect 1/2<111> dislocation loop can be clearly observed by MD calculations, and their lifetime is largely dependent on the temperature and cluster size. To clarify this point, we examined the probability of sessile structure formation (up to 1 ns) via the interaction of two 1/2<111> loops with equal size at different temperatures. As illustrated in Fig. 3a, the formation probability of sessile complexes reaches up to 100 % at low temperatures, but decreases sharply at moderate temperatures, regardless of the cluster size of reacting loops. With a further increase in temperature, it is essentially impossible to obtain the sessile complex in bcc Fe (up to the reaction of two 91-SIAs clusters), which will transform into a parallel dislocation loop along <111> directions within 1 ns of simulation. Moreover, similar to previous studies [42], the increase of reacting loop size also promotes the probability of sessile complex formation due to the increment of junction length, from 10 % for 37-37 reaction to 100 % for 91-91 reaction at 800 K. Besides the temperature, the size difference between two loops also has a profound impact on the results of bi-loop reactions. As displayed in Fig. 3b, the probability of sessile complex formation monotonically decreases with the increasing of size difference, from 100 %/70 %/10 % for 91-91/61-61/37-37 (i.e., the size difference of 0 %) reactions to 50 %/0 %/0 % for 64–91/43-61/26–37 (i.e., the size difference of 30 %) reactions.

The above results suggest that the interaction of two gliding 1/2<111> dislocation loops in bcc Fe will induce either the formation of a sessile complex containing differently orientated SIAs or the formation of a perfect glissile loop consisting of parallel SIAs. The former is in fact unstable and can easily transform into a glissile loop, especially at high temperatures or with a significant size difference between the two reacting loops. Therefore, the direct formation of a <100>-type dislocation loop through bi-loop reactions in strain-free Fe seems impossible in our simulations. This is consistent with previous studies by Marian et al. [18], but somewhat different from that reported by Xu et al. [5] that observed the <100> loop formation through interactions of two 1/2<111> loops. Such discrepancy should be attributed to the different interatomic potentials. The Fe-Fe potential developed by Ackland et al. [45] was used in the present work and Terentyev et al. [42], while Xu et al. selected the interatomic potential developed by Marlerba et al. [46]. It is important to note that the relative stability of 1/2<111> and <100> loops obtained by Marlerba's potential is contrary to that predicted by other potentials and first-principle calculations [18,19,51,52], and thus may overestimate the formation probability of <100>

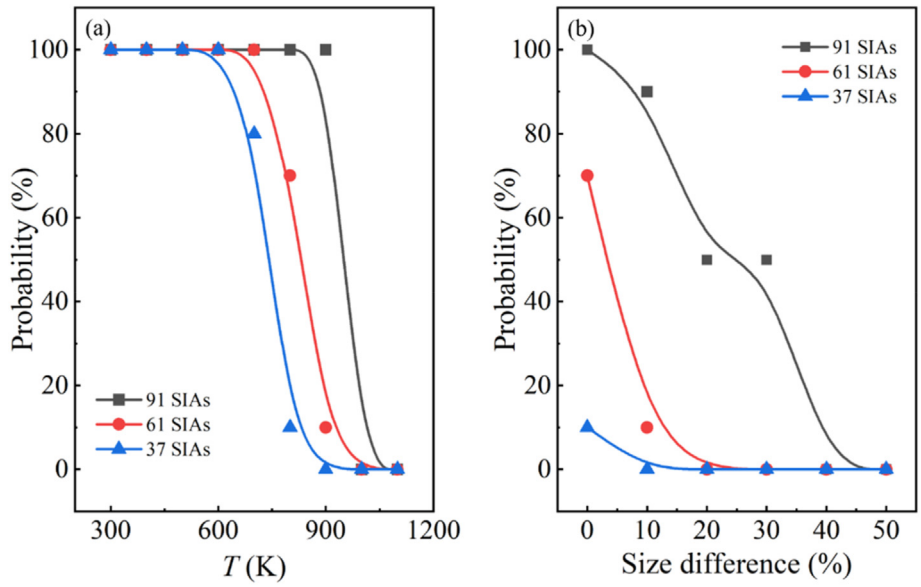

Fig. 3. Formation probability of sessile complexes in relation to (a) temperature and (b) size difference: (a) the reaction of two loops of equal size at different temperatures, (b) the reaction of loops with varied sizes at 800 K. The size difference is obtained by $(N_{large} - N_{small})/N_{large}$, where N_{large} and N_{small} represent the number of SIAs in the larger and smaller loops, respectively. Here, 91 SIAs, 61 SIAs, and 37 SIAs represent the larger loops. Each case was calculated 10 times for repetition.

dislocation loops.

3.2. Influence of strain on the interaction between two 1/2<111> loops

Physically, the presence of strain/stress may significantly affect the thermodynamic and kinetic behaviors of SIA clusters in materials due to the strong coupling of lattice distortion induced by SIAs with the external/internal stress field [34,36]. This is particularly important for damaged materials, because there is distinct out-of-surface swelling of the crystal lattice owing to high-energy particle irradiation [53,54]. However, how such lattice strain affects the interaction of two gliding 1/2<111> dislocation loops as well as the formation of <100> loops is still unclear and remains to be elucidated. Here, taking uniaxial strain as an example, we investigated the strain-dependent bi-loop reactions in bcc Fe.

3.2.1. Formation of <100> dislocation loops under uniaxial strain

The most striking result to emerge from the interaction of two dislocation loops in strained Fe is the occurrence of <100>-type loops, which cannot be observed under strain-free conditions. Therefore, we further calculated the formation probability of <100> loops through the reaction of two equal-sized 1/2<111> loops (~61 SIAs) at different temperatures and strains (up to 1 ns). Since different structures in the final state can be obtained from the beginning of identical initial configurations, indicating the stochastic dynamical processes of bi-loop reactions in nature, the calculations for each case were repeated 10 times. It should be noted that, due to the structural anisotropy of dislocation interactions, the results of bi-loop reactions also depend on the orientation of the applied strain, and thus two different uniaxial directions were taken into account, including *x*-axis (i.e., [100] direction) and *z*-axis (i.e., [001] direction) strain.

As shown in Fig. 4a, the applied uniaxial strain along *x*-axis can substantially increase the probability of <100> loop formation,

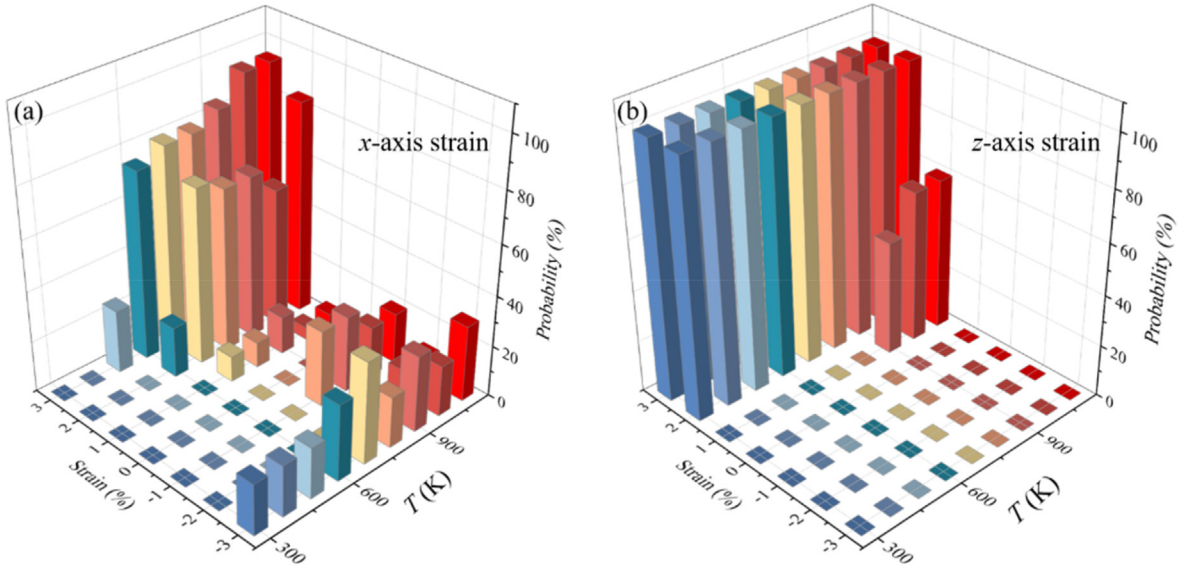

Fig. 4. The probability of <100> loop formation from bi-loop reactions under different conditions: (a) strain applied along the x-axis, (b) strain applied along the z-axis.

regardless of the sign of uniaxial strain, but the enhancing effects of tensile strain are stronger than those of compressive strain. For example, the probability of <100> loop formation at 1100 K can reach up to 95 % under 3 % tensile strain, while that is only 30 % under 3 % compressive strain. For the cases with the same strained conditions, the increase of temperature generally induces the increment of formation probability of <100> loops, from 0 %/20 % at 300 K to 95 %/30 % at 1100 K under 3 %/-3 % uniaxial strain along *x*-axis. This is due to the fact that, as discussed in the following sections, the generation of <100> dislocation loops via bi-loop reaction is a thermal-activated event, and can be promoted by temperature increment. Moreover, the probabilities of <100> loop formation under uniaxial strain along *x*-axis are substantially different from that of strain along *z*-axis, confirming the key role of strain orientation on the results of loop-loop interactions in bcc Fe. As shown in Fig. 4b, there is no < 100> loop observation under compressive strain along *z*-axis, while its formation probability can reach up to 100 % when the tensile strain is larger than 2 %. Therefore, the presence of external strain can effectively promote the formation probability of <100>-type dislocation loops via the interaction of two gliding 1/2<111> loops in Fe, especially for cases with tensile strain. It is important to note that the enhancing effect of uniaxial strain on the generation of <100> loops is almost independent of the interatomic potentials, except for the exact value of the formation probability. For instance, under 3 % strain along the *x*-axis, the formation probabilities of <100> loops are 60 %, 80 %, and 100 % for the A97 [47], M03 [48], and M07 [46] potentials, respectively.

Next, we presented the detailed descriptions and examples of each microscopic process observed during bi-loop reactions. Generally, the formation processes of <100> loops in strained Fe can be categorized into two different modes. The first is the *coplanar* mode and mainly occurs when the external uniaxial strain is applied along the *x*-axis (ranging from −1 % to 3 %). In contrast, when tensile strain is applied along the *z*-axis or a large compressive strain (ranging from −3 % to −1 %) is applied along the *x*-axis, a simple *non-coplanar* mode dominates the evolution process. For the *coplanar* mode, as displayed in Fig. 5a and b, the sessile structures containing a junction line and SIAs along [001] direction are formed in strained Fe at the beginning of a 1/2<111> dislocation loop encountering another one. This is in good agreement with that in strain-free conditions (see Fig. 2) and conserves the Burgers vectors. However, different from a quick transformation into a perfect glissile loop in strain-free Fe, the lifetime of the sessile cluster under uniaxial strain is significantly increased, enabling the interactions of SIAs and leading to the long-term evolution of loop structures. After that, the junction line with a [001] dislocation segment will split into two screw dislocations with Burgers vectors of $1/2[\bar{1}1\bar{1}]$ and $1/2[1\bar{1}\bar{1}]$, as illustrated in Fig. 5a and b. From this point, the mixed loop continues to evolve by the growth of screw segments, leading to the formation of a critical configuration in which about one third of SIAs in the dislocation loop adopts the $1/2[\bar{1}\bar{1}1]$ orientation, the last third of SIAs has a 1/2[111] orientation, and the middle third consists of SIAs along [100] or [010] directions. With further evolution of SIAs, the fraction of [100] or [010] loops grows gradually, resulting in the formation of a perfect [100] or [010] dislocation loop (see process 4 in Fig. 5a and b). Intriguingly, this is different from the prediction (~[001] orientation) from conventional dislocation reaction theory, in which the Burgers vectors are conserved.

As for the *non-coplanar* mode, its reaction processes are relatively simple. The junction line consisting of SIAs along the [001] direction is also formed at the initial stage, but other defects are located on different planes, corresponding to a three-dimensional configuration (see process 5 in Fig. 5c and d). In addition, this intermediate [001] loop continues to grow via the interaction between SIAs along $1/2[\bar{1}\bar{1}1]$ and 1/2[111] directions, finally leading to the formation of a pure [001] dislocation loop. Note that the entire evolution process of the bi-loop reaction in the *non-coplanar* mode obeys Kirchhoff's law and maintains the conservation of Burgers vector.

3.2.2. Activation energy barriers of each reaction process for <100> loop formation

The above results explicitly demonstrate that the formation of <100> dislocation loops via bi-loop reaction is a complicated atomistic process in strained bcc Fe, which involves the coordinated movement and/or rearrangement of multiple interstitials in several intermediate configurations. Thus, based on the microscopic evolution observed, we further examined the activation energy of these processes as well as the stability of the products during the interaction of two gliding 1/2<111> loops. Here, two different ways are used to determine the activation energy barriers, including the direct calculation using the NEB method and derivation from the Arrhenius formula (time of <100> loop formation vs temperature). The former is used to calculate the energy barrier for each reaction process, while the latter can be employed to evaluate the effective energy barrier for whole reactions.

Fig. 6 shows the activation energy barriers of each reaction during <100> loop formation via loop-loop interactions in bcc Fe. In order to clarify the influence of anisotropic strain on the kinetic processes, the tensile uniaxial strains along both *x*- and *z*-axes are considered, corresponding to the *coplanar* and *non-coplanar* mode respectively. The cases of compressive strain along the *x*-axis are excluded in our calculations, because it will induce tensile strain in the *y*- and *z*-axes owing to the Poisson effect, thereby equivalent to the former two cases. It is important to note that all intermediate states are obtained by the calculations of 3 % tensile strain along *x*-axis (*coplanar* mode) or *z*-axis (*non-coplanar* mode). Afterward, the strain conditions for these intermediate states are changed accordingly without variation of relative atomic positions, and NEB calculations are then conducted. As displayed in Fig. 6a, the activation energy barriers without strain can reach up to 2.70/1.02/1.07/0.95 eV for the process 1/2/3/4 in *coplanar* mode. Such high values confirm the low probability of <100> loop formation via bi-loop reaction in strain-free Fe, and the maximum energy barrier occurs for splitting a [001] dislocation segment into two screw dislocations (see process 1 in Fig. 5a). More importantly, the external strain significantly reduces the energy barrier of this reaction, from 2.70 eV without strain to 1.28/0.53/0.37 eV under uniaxial tensile strain of 1 %/2 %/3 %, which suggests that the uniaxial strain enhances the nucleation of screw dislocation segments. This strain-induced reduction of activation energy barrier can also be observed for other reaction processes, as shown in Fig. 6a, and thus promotes the generation of <100> dislocation loops in *coplanar* mode. Intriguingly, the reaction of the maximum activation energy transforms from process 1 without strain to process 4 (the growth of the [100] loop, see Fig. 5a) under tensile strain along *x*-axis, and the effective energy barrier decreases from 2.70 eV in strain-free Fe to 0.64 eV with 3 % tensile strain.

Similar results are also obtained for the <100> loop formation in *non-coplanar* mode. As illustrated in Fig. 6b, the activation energy barrier of process 5 equals zero, regardless of the external strain, implying that the formation of a three-dimensional configuration for the mixed structure containing a [001] junction line (see process 5 in Fig. 5c) is a barrier-free process and may occur spontaneously. Thus, the formation probability of <100> loops in *non-coplanar* mode is mainly dependent on the activation energy barrier of continuous growth of [001] segregation (see process 6 in Fig. 5c). This is calculated to be 2.67 eV in strain-free Fe, as displayed in Fig. 6b, and decreases with the increasing tensile strain along the *z*-axis, from 1.09 eV with 1 % strain to approximately 0 eV with 2 % or 3 % strain. These results are consistent with the formation probability of <100> loop in Fe under uniaxial strain along *z*-axis (see Fig. 4b), because it can reach up to 100 % when the tensile strain is larger than 2 %.

Although the NEB calculations provide a direct evaluation of activation energy for each reaction process, the accuracy of their results is closely related to the artificial selection of intermediate states. Hence, to comprehensively assess the effective energy barrier of <100> loop formation, we also examined the evolution time required for the generation of a pure <100> loop as a function of simulation temperature, as shown in Fig. 7. It is clear that the increase of temperature can dramatically

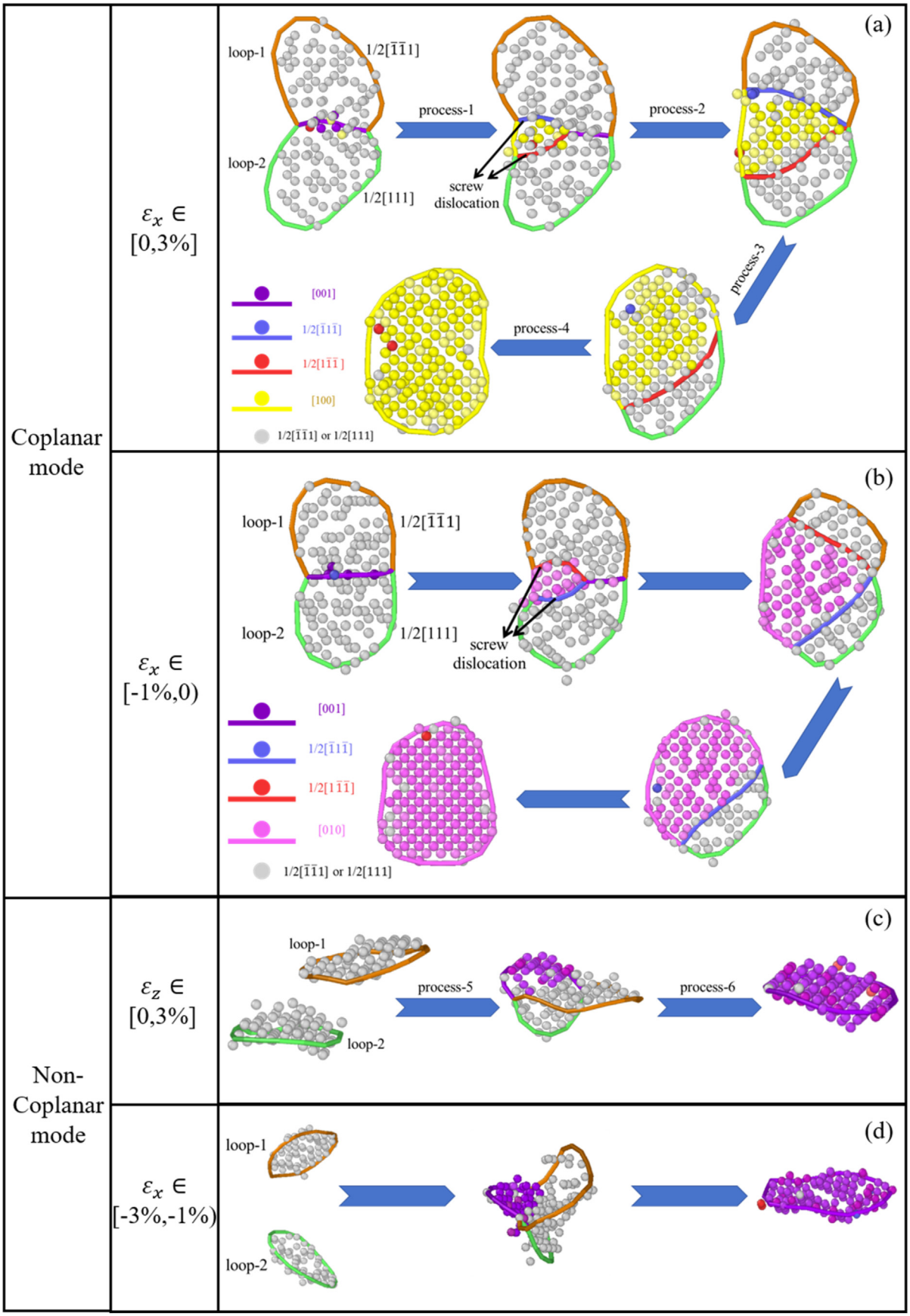

Fig. 5. Reaction processes of the bi-loop reaction under different modes at 800K. The legend shows the direction of SIAs (spheres) and Burgers vector of dislocation (lines).

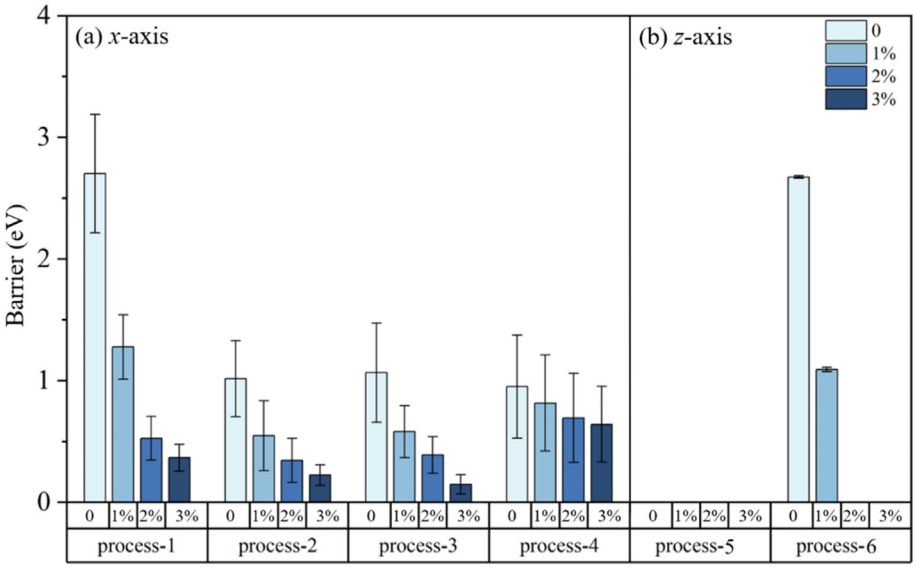

Fig. 6. The energy barriers for each stage in bi-loop reaction under uniaxial tensile strain: (a) strain applied along the *x*-axis, (b) strain applied along the *z*-axis. Note that the atomic configurations of 0/1 %/2 % are derived from the direct dimensional transformation of the atomic configuration of 3 %. The reaction processes are denoted in Fig. 5.

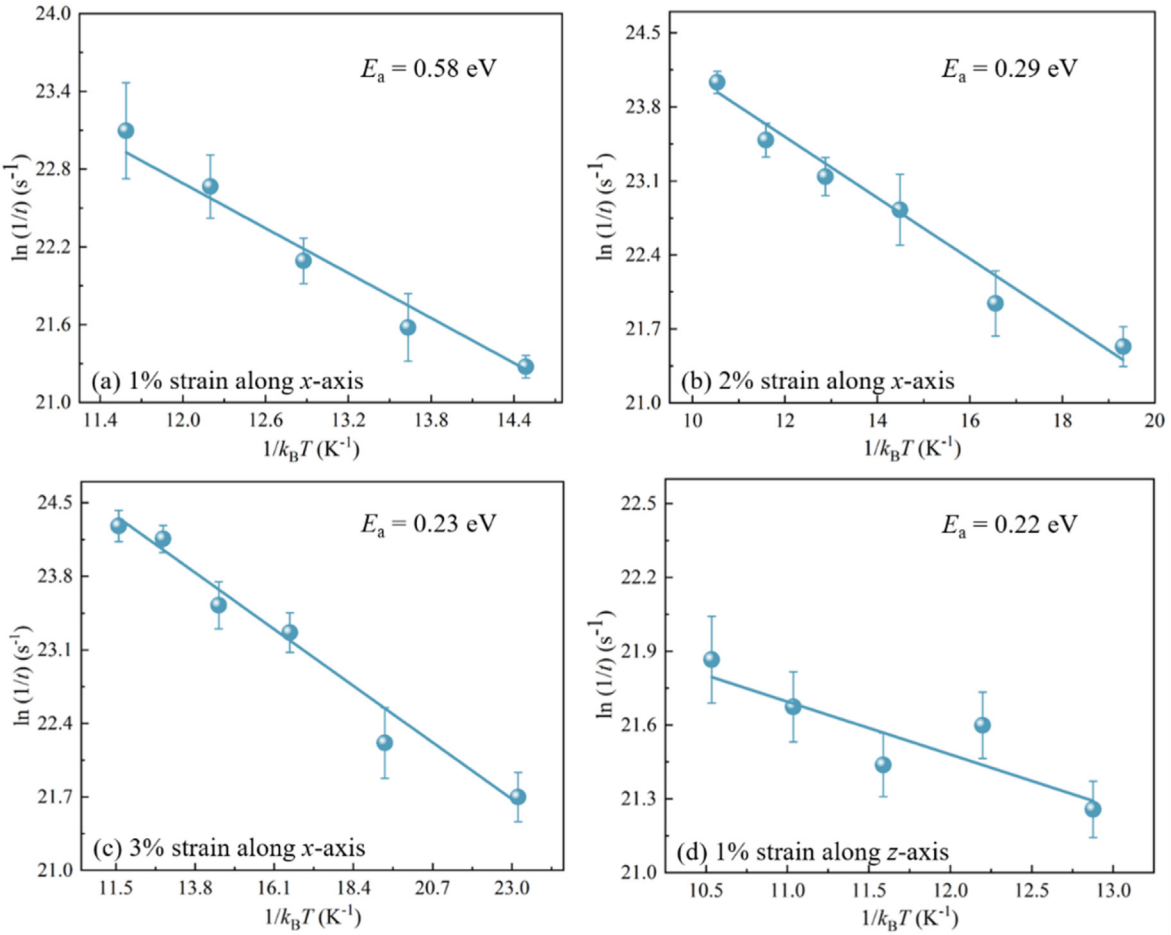

Fig. 7. The time required to form a complete <100> loop in bi-loop reaction at different temperatures: (a) 1 % strain applied along the x-axis, (b) 2 % strain applied along the x-axis, (c) 3 % strain applied along the x-axis, (d) 1 % strain applied along the z-axis. Results are obtained by reaction of two equal-sized 1/2<111> loops (~61 SIAs).

accelerate the reactions of two gliding dislocation loops as well as the formation of the <100> loop, verifying that this is a thermal-activated event. Accordingly, the correlation between occurrence time t and temperature T can be well described by the Arrhenius formula

$$\ln\frac{1}{t} = \ln A - \frac{E_a}{k_B T}, \tag{1}$$

where A is a constant and represents the attempt frequency. E_a and k_B denote the activation energy barrier and Boltzmann constant, respectively. Based on this equation and MD simulations, the effective energy barrier of bi-loop reactions in strained Fe can be obtained. As displayed in Fig. 7, the activation energy of <100> loop formation is calculated to be 0.58 eV with 1 % uniaxial tensile strain applied along *x*-axis, which further decreases with the increasing tensile strain, i.e., 0.29 eV for 2 % strain and 0.23 eV for 3 % strain. For the case of *non-coplanar* mode (i.e., external tensile strain applied along the *z*-axis), the estimated activation energy barrier is 0.22 eV under 1 % tensile strain, as shown in Fig. 7d. It should be noted that the time-temperature correlation for 2 % or 3 % tensile strain along the *z*-axis does not follow the Arrhenius equation, suggesting that it is a barrier-free process and consistent with the NEB results (see Fig. 6b), and thus the corresponding energy barriers are not presented. Specifically, the energy barriers derived from Eq. (1) are somewhat lower than that of NEB calculations, which should be attributed to the artificial selection of reaction paths, leading to the slight discrepancy in activation energy between the two different methods.

3.3. Influence of size difference on the formation of <100> loop

As mentioned in Section 3.1, the detailed processes of loop-loop interactions are largely dependent on their size difference. Thus, we further investigated the influence of size difference on the probability of <100> loop formation under strained conditions. Here, we considered three standard sizes of dislocation loops in our calculations, including 37 SIAs, 61 SIAs and 91 SIAs, while the size of the other loop (N) is smaller than the standard loop (N_{std}), and the relative difference is given by (N_{std}-N)/N_{std}. It should be noted that in comparison with the absolute values of loop sizes, their relative difference plays a dominant role in the size effects.

Fig. 8 shows the probability of <100> loop formation at 800 K as a function of relative size difference (standard size of 91 SIAs) and external uniaxial strain. Note that only the results under tensile strain are presented, because the influence of compressive strain along the *x*-axis is equivalent to that of tensile strain along the *y*- and *z*-axes. As expected, both the increase in size difference and the decrease in tensile strain significantly suppress the generation of <100> loops via bi-loop reactions in bcc Fe. For example, the probability of <100> loop formation under 3 % tensile strain along *x*-axis can reach up to 100 % with two equal-sized loops (e.g., 91-91), while that is reduced to 0 % with a size difference of 40 % (e.g., 55–91). Specifically, a considerable formation probability (~40 %) of <100> loops can still be obtained under 2 % or 3 % tensile strain along the *z*-axis with a relative size difference of 50 %, as shown in Fig. 8b. These results are completely different from the previous study on strain-free Fe by Xu et al. [5], in which the formation of a <100> loop via bi-loop reactions only occurs when the sizes of the two gliding 1/2<111> loops are identical. The probability of <100> loop formation is higher for uniaxial tensile strain applied along the *z*-axis compared to the *x*-axis. This is consistent with the kinetic reactions for <100> loop formation, which is a barrier-free process as long as the tensile strain applied along the *z*-axis is greater than 1 % (see Fig. 6b).

Based on the results mentioned above, we developed a predictive model to describe the variation in formation probability under different strain conditions and relative size differences, i.e.,

$$p = \frac{a \cdot \exp\left(b \cdot S_{diff} + c \cdot \varepsilon\right)}{1 + a \cdot \exp\left(b \cdot S_{diff} + c \cdot \varepsilon\right)}, \tag{2}$$

where S_{diff} is the relative size difference between two reacting loops and ε denotes the uniaxial strain; *a, b* and *c* represent the fitting parameters as displayed in Table 1.

To further comprehensively evaluate the performance of this predictive model, we calculated two different error functions: the Pearson correlation coefficient r and the determination coefficient R^2, which can be expressed as [55,56].

$$r = \frac{\sum_{i=1}^{n}(\hat{y}_i - \overline{\hat{y}_i})(y_i - \bar{y})}{\sqrt{\sum_{i=1}^{n}(\hat{y}_i - \overline{\hat{y}_i})^2}\sqrt{\sum_{i=1}^{n}(y_i - \bar{y})^2}}, \tag{3}$$

Table 1
Fitting parameters of the predictive model.

	a	b	c
ε_x	0.056	−13.74	192.73
ε_z	0.177	−7.35	183.76

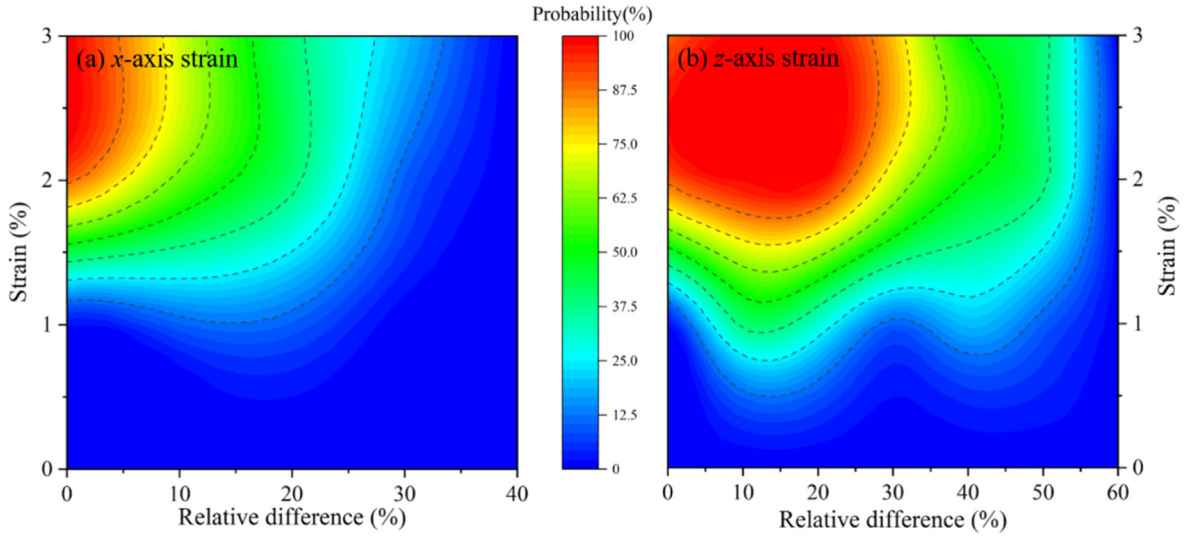

Fig. 8. The probability of <100> loop formation in reactions with varied loop sizes at 800K: (a) strain applied along the x-axis, (b) strain applied along the *z*-axis.

$$R^2 = 1 - \frac{\sum_i (\hat{y}_i - y_i)^2}{\sum_i (y_i - \bar{y})^2}, \quad (4)$$

where $\hat{y}_i$ and y_i are the predicted and true values of the data points, while $\overline{\hat{y}_i}$ and $\bar{y}$ represent the mean values of the predicted and true values, respectively; n is the number of data points. Fig. 9 shows the formation probability of <100> loops in strained Fe obtained by both model prediction and MD calculations. Note that the data displayed in Fig. 9 also includes the results for other standard sizes (i.e., 37 and 61 SIAs) of reacting loops. As shown in Fig. 9, most points lie on the line of x=y, suggesting that the results derived from the predictive model (x coordinates) are consistent with those obtained by MD simulations (y coordinates). Furthermore, the error functions are calculated to be 0.94 for Pearson correlation coefficient and 0.88 for determination coefficient. These values, in combination with the good agreement of formation probability between model predictions and direct calculations, further verify the availability and accuracy of the predictive model.

3.4. Comparison with experimental observations

Dislocation loops, as the typical product of high-energy particle irradiation, have a profound impact on the microstructural evolution and thermo-mechanical properties of materials. Intriguingly, both 1/2<111> and <100> type dislocation loops were clearly identified in bcc metals [6,10–17]. Because of the extremely low mobility of <100> loops, they can serve as stationary sinks for displacement defects and strong obstacles for edge dislocations, thus affecting the response of materials to irradiation [9,57]. Since it is generally accepted that the stability of 1/2<111> loop is much higher than that of <100> loop in bcc metals, the underlying physics of <100> loop formation in irradiated Fe is still unclear and controversies abound in the literature.

Herein, taking bcc Fe as an example, our calculations suggest that, although there is no < 100> loop occurrence via the reaction of two gliding 1/2<111> loops under strain-free conditions, the external anisotropic strain significantly enhances the formation of <100> loop. This is completely different from the dislocation reaction mechanisms proposed previously [5,18,33], in which some stringent conditions are required for the topology and size of the reacting loops (e.g., two equal-sized loops with an acute angle [5,18] or coalescence of multiple loops simultaneously [33]), and thus provides a reasonable interpretation for the frequent occurrence of <100> loops. For example, even when the relative size difference between two reactant loops is as much as 50 %, the formation probability (~40 %) of <100> loops is still considerable under 3 % uniaxial tensile strain. These results are in good agreement with the experimental observations [16], where the reaction of two 1/2<111> loops with different sizes (6.1 nm and 12.5 nm) induces the formation of a larger <100> loop. It is important to note that the loop-loop interactions in strained Fe are thermal-activated events and stochastic in nature, leading to distinct products from identical initial configurations. Therefore, the activation energy barriers of each reaction step for <100> loop formation are determined and generally decreases with the increase in uniaxial strain. More importantly, we developed a predictive model to describe the formation probability of <100> loops under different strain conditions and relative size differences, which can be integrated into large-scale simulations (e.g., cluster dynamics and kinetic Monte Carlo), enabling multiscale simulations to assess the evolution of irradiation damage in Fe-based materials.

In addition, numerous experimental studies were conducted to identify several key factors in determining the relative fraction of <100> loops in Fe, including the irradiation temperature [13,23,38], chromium (Cr) content [40] and stress [35,37]. For example, Yao et al. [23] found that the fraction of <100> loops generally increases with increasing temperatures, and almost exclusively <100> dislocation loops were observed at high temperatures (>773 K). This trend is in good agreement with our simulations, because the temperature increment induces an obvious probability increase of <100> loop formation via bi-loop reactions in strained Fe (see Fig. 4). In addition, the presence of Cr will reduce the relative fraction of <100> loops in irradiated Fe-Cr alloys [40]. This may be attributed to the strong attractive interaction between Cr and 1/2<111> loops [40,57,58], which significantly suppresses the migration of 1/2<111> loops and reduces the probability of loop-loop reactions, and thus is detrimental to the generation of <100> loops. More importantly, Xu et al. [35] investigated the dislocation loop distribution in stress-loaded (uniaxial tensile stress of 100–200 MPa) T91 steel after 3 MeV proton irradiation (~1 or 2 dpa). It is found that most <100> loops are preferentially formed in the tensile directions, and the anisotropy of dislocation loops (positive correlation to <100> loops) monotonically increases with increasing applied uniaxial stress. These experimental observations are consistent with our simulations, in which the direction of <100> loops and the anisotropy of final products are closely related to the direction of uniaxial strain (see Fig. 4).

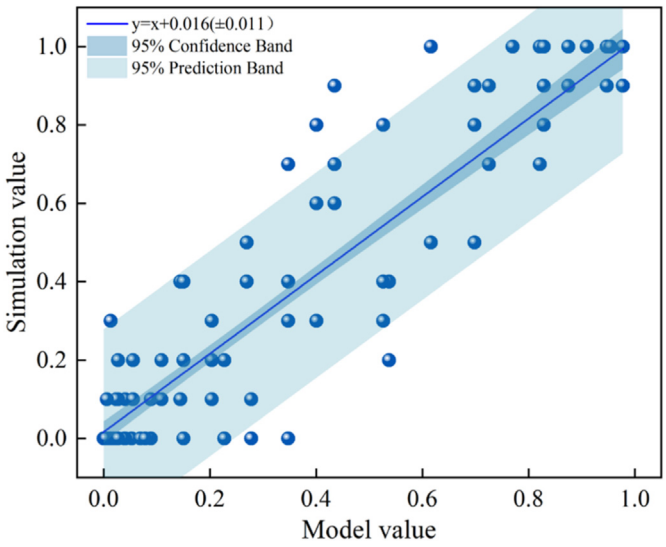

Fig. 9. Comparison between model predictions and simulation results.

4. Conclusion

In present work, we have systematically investigated the influence of anisotropic strain on the interaction between two gliding 1/2<111> dislocation loops as well as the formation of <100> loops in bcc Fe through molecular dynamics and statistics simulations. The main conclusions are summarized as follows.

(1) It is found that there is no < 100> loop formation via the bi-loop reactions in strain-free Fe, even for the cases of two reactant loops with equal size. However, the presence of uniaxial strain significantly promotes the generation of <100> loops via loop-loop interaction, and their formation maintains a considerable probability under 3 % tensile strain even when the relative size difference can reach up to 50 %. A predictive model is proposed to describe the formation probability of <100> loops under different conditions.

(2) Two different microscopic mechanisms of <100> loop formation, i.e., coplanar mode and non-coplanar mode, are proposed, and both of them are a complicated evolution and involve the coordinated movement and/or the rearrangement of multiple interstitials in several intermediate configurations. Intriguingly, the Burgers vectors of dislocation loops before and after coplanar reactions are not conserved, which is different from the conventional reaction mechanism.

(3) As a thermal-activated event and stochastic in nature, the activation energy barriers of <100> loop formation through bi-loop reactions are calculated, and they decrease with the increasing uniaxial strain. Our findings advocate the critical role of anisotropic strain on the bi-loop reaction and <100> loop formation, and provide an essential predictive tool for assessing the irradiation damage evolution in bcc metals.

CRediT authorship contribution statement

Hong-Bo Zhou: Writing – review & editing, Supervision, Project administration, Funding acquisition, Formal analysis, Conceptualization. **Xin-Ya Tang:** Writing – original draft, Investigation, Formal analysis, Data curation. **Yu-Hao Li:** Writing – review & editing, Methodology, Investigation, Formal analysis. **Tian-Ren Yang:** Validation, Formal analysis. **Hao-Xuan Huang:** Validation, Software, Formal analysis. **Qing-Yuan Ren:** Formal analysis. **Guang-Hong Lu:** Writing – review & editing, Supervision, Formal analysis.

Declaration of competing interest

The authors declare that they have no known competing financial interests or personal relationships that could have appeared to influence the work reported in this paper.

Acknowledgement

This work was financially supported by the National Natural Science Foundation of China (Grant Nos. 12192281 and 12075022).

References

[1] B.D. Wirth, How does radiation damage materials? Science 318 (2007) 923–924, https://doi.org/10.1126/science.1150394.
[2] J. Zhang, Jirigalantu, S. Yu, Y. Wang, H. Yu, W. Li, Research on manufacturing technology of nanoimprinted grating, J. Manuf. Process. 131 (2024) 891–909, https://doi.org/10.1016/j.jmapro.2024.09.033.
[3] S.J. Zinkle, G.S. Was, Materials challenges in nuclear energy, Acta Mater. 61 (2013) 735–758, https://doi.org/10.1016/j.actamat.2012.11.004.
[4] P. Yvon, F. Carré, Structural materials challenges for advanced reactor systems, J. Nucl. Mater. 385 (2009) 217–222, https://doi.org/10.1016/j.jnucmat.2008.11.026.
[5] H. Xu, R.E. Stoller, Y.N. Osetsky, D. Terentyev, Solving the puzzle of <100> interstitial loop formation in bcc iron, Phys. Rev. Lett. 110 (2013) 265503, https://doi.org/10.1103/PhysRevLett.110.265503.
[6] J.C. Haley, S.A. Briggs, P.D. Edmondson, K. Sridharan, S.G. Roberts, S. Lozano-Perez, K.G. Field, Dislocation loop evolution during in-situ ion irradiation of model FeCrAl alloys, Acta Mater. 136 (2017) 390–401, https://doi.org/10.1016/j.actamat.2017.07.011.
[7] D. Brimbal, B. Décamps, A. Barbu, E. Meslin, J. Henry, Dual-beam irradiation of α-iron: heterogeneous bubble formation on dislocation loops, J. Nucl. Mater. 418 (2011) 313–315, https://doi.org/10.1016/j.jnucmat.2011.06.048.
[8] F. Li, Y. Wei, F. Luo, W. Zhang, X. Zhou, Y. Chen, C. Chen, L. Guo, J. Xin, S. Mo, Behaviors of bubble-loop complexes in He-irradiated CLAM steels at elevated temperatures, J. Nucl. Mater. 529 (2020) 151954, https://doi.org/10.1016/j.jnucmat.2019.151954.
[9] G. Bonny, D. Terentyev, J. Elena, A. Zinovev, B. Minov, E.E. Zhurkin, Assessment of hardening due to dislocation loops in bcc iron: overview and analysis of atomistic simulations for edge dislocations, J. Nucl. Mater. 473 (2016) 283–289, https://doi.org/10.1016/j.jnucmat.2016.02.031.
[10] X. Yi, M.L. Jenkins, M. Briceno, S.G. Roberts, Z. Zhou, M.A. Kirk, In situ study of self-ion irradiation damage in W and W-5Re at 500 °C, Philos. Mag. 93 (2013) 1715–1738, https://doi.org/10.1080/14786435.2012.754110.
[11] W.-Y. Chen, Y. Miao, J. Gan, M.A. Okuniewski, S.A. Maloy, J.F. Stubbins, Neutron irradiation effects in Fe and Fe-Cr at 300 °C, Acta Mater. 111 (2016) 407–416, https://doi.org/10.1016/j.actamat.2016.03.060.
[12] X. Yi, M.L. Jenkins, M.A. Kirk, Z. Zhou, S.G. Roberts, In-situ TEM studies of 150 keV W^+ ion irradiated W and W-alloys: damage production and microstructural evolution, Acta Mater. 112 (2016) 105–120, https://doi.org/10.1016/j.actamat.2016.03.051.
[13] R. Schäublin, B. Décamps, A. Prokhodtseva, J.F. Löffler, On the origin of primary 1/2a_0 <111> and a_0<100> loops in irradiated Fe(Cr) alloys, Acta Mater. 133 (2017) 427–439, https://doi.org/10.1016/j.actamat.2017.02.041.
[14] Y. Li, G. Ran, Y. Guo, Z. Sun, X. Liu, Y. Li, X. Qiu, Y. Xin, The evolution of dislocation loop and its interaction with pre-existing dislocation in He^+-irradiated molybdenum: in-situ TEM observation and molecular dynamics simulation, Acta Mater. 201 (2020) 462–476, https://doi.org/10.1016/j.actamat.2020.10.022.
[15] Y. Li, L. Wang, G. Ran, Y. Yuan, L. Wu, X. Liu, X. Qiu, Z. Sun, Y. Ding, Q. Han, X. Wu, H. Deng, X. Huang, In-situ TEM investigation of 30 keV he^+ irradiated tungsten: effects of temperature, fluence, and sample thickness on dislocation loop evolution, Acta Mater. 206 (2021) 116618, https://doi.org/10.1016/j.actamat.2020.116618.
[16] Y. Li, G. Ran, X. Liu, Q. Han, X. Huang, Y. Ding, In-situ TEM investigation of dislocation loop reaction and irradiation hardening in H_2^+-He^+ dual-beam irradiated Mo, J. Mater. Sci. Technol. 107 (2022) 14–25, https://doi.org/10.1016/j.jmst.2021.07.040.
[17] M. Wu, J. Huang, Z. Cao, Y. Ding, Q. Zhong, Y. Zhao, G. Ran, Effect of hydrogen, helium and dose rate on the evolution of dislocation loop in pure iron during in-situ ion irradiation, J. Nucl. Mater. 598 (2024) 155161, https://doi.org/10.1016/j.jnucmat.2024.155161.
[18] J. Marian, B.D. Wirth, J.M. Perlado, Mechanism of formation and growth of <100> interstitial loops in ferritic materials, Phys. Rev. Lett. 88 (2002) 255507, https://doi.org/10.1103/PhysRevLett.88.255507.
[19] J. Chen, N. Gao, P. Jung, T. Sauvage, A new mechanism of loop formation and transformation in bcc iron without dislocation reaction, J. Nucl. Mater. 441 (2013) 216–221, https://doi.org/10.1016/j.jnucmat.2013.05.074.
[20] J. Gao, K. Yabuuchi, A. Kimura, Ion-irradiation hardening and microstructural evolution in F82H and ferritic alloys, J. Nucl. Mater. 515 (2019) 294–302, https://doi.org/10.1016/j.jnucmat.2018.12.047.
[21] B.L. Eyre, R. Bullough, On the formation of interstitial loops in b.c.c. metals, Philos. Mag. 12 (1965) 31–39, https://doi.org/10.1080/14786436508224943.
[22] S.L. Dudarev, R. Bullough, P.M. Derlet, Effect of the α-γ phase transition on the stability of dislocation loops in bcc iron, Phys. Rev. Lett. 100 (2008) 135503, https://doi.org/10.1103/PhysRevLett.100.135503.
[23] Z. Yao, M.L. Jenkins, M. Hernández-Mayoral, M.A. Kirk, The temperature dependence of heavy-ion damage in iron: a microstructural transition at elevated temperatures, Philos. Mag. 90 (2010) 4623–4634, https://doi.org/10.1080/14786430903430981.
[24] D. Brimbal, B. Décamps, J. Henry, E. Meslin, A. Barbu, Single- and dual-beam in situ irradiations of high-purity iron in a transmission electron microscope: effects of heavy ion irradiation and helium injection, Acta Mater. 64 (2014) 391–401, https://doi.org/10.1016/j.actamat.2013.10.052.
[25] B.C. Masters, Dislocation loops in irradiated iron, Philos. Mag. 11 (1965) 881–893, https://doi.org/10.1080/14786436508223952.
[26] A. Chartier, M.C. Marinica, Rearrangement of interstitial defects in alpha-Fe under extreme condition, Acta Mater. 180 (2019) 141–148, https://doi.org/10.1016/j.actamat.2019.09.007.
[27] Y. Zhang, X.-M. Bai, M.R. Tonks, S.B. Biner, Formation of prismatic loops from C15 Laves phase interstitial clusters in body-centered cubic iron, Scr. Mater. 98 (2015) 5–8, https://doi.org/10.1016/j.scriptamat.2014.10.033.
[28] A.F. Calder, D.J. Bacon, A.V. Barashev, Y.N. Osetsky, On the origin of large interstitial clusters in displacement cascades, Philos. Mag. 90 (2010) 863–884, https://doi.org/10.1080/14786430903117141.
[29] F. Granberg, J. Byggmästar, A.E. Sand, K. Nordlund, Cascade debris overlap mechanism of <100> dislocation loop formation in Fe and FeCr, Europhys. Lett. 119 (2017) 56003, https://doi.org/10.1209/0295-5075/119/56003.
[30] Q. Peng, F. Meng, Y. Yang, C. Lu, H. Deng, L. Wang, S. De, F. Gao, Shockwave generates <100> dislocation loops in bcc iron, Nat. Commun. 9 (2018) 4880, https://doi.org/10.1038/s41467-018-07102-3.
[31] A.F. Calder, D.J. Bacon, A.V. Barashev, Y.N. Osetsky, Effect of mass of the primary knock-on atom on displacement cascade debris in α-iron, Philos. Mag. Lett. 88 (2008) 43–53, https://doi.org/10.1080/09500830701733004.
[32] O. El-Atwani, W.S. Cunningham, J.R. Trelewicz, M. Li, B.D. Wirth, S.A. Maloy, Revealing the synergistic effects of sequential and simultaneous dual beam irradiations in tungsten via in-situ TEM, J. Nucl. Mater. 538 (2020) 152150, https://doi.org/10.1016/j.jnucmat.2020.152150.
[33] X. Wang, N. Gao, Y. Wang, X. Wu, G. Shu, C. Li, Q. Li, B. Xu, W. Liu, Formation of <100> dislocation loop in bcc-Fe via the ternary loop reaction, Scr. Mater. 162 (2019) 204–208, https://doi.org/10.1016/j.scriptamat.2018.11.002.
[34] Z. Chen, N. Kioussis, N. Ghoniem, D. Seif, Strain-field effects on the formation and migration energies of self interstitials in α-Fe from first principles, Phys. Rev. B 81 (2010) 094102, https://doi.org/10.1103/PhysRevB.81.094102.
[35] C. Xu, G.S. Was, Anisotropic dislocation loop distribution in alloy T91 during irradiation creep, J. Nucl. Mater. 454 (2014) 255–264, https://doi.org/10.1016/j.jnucmat.2014.07.062.
[36] C. Kang, Q. Wang, L. Shao, Kinetics of interstitial defects in α-Fe: the effect from uniaxial stress, J. Nucl. Mater. 485 (2017) 159–168, https://doi.org/10.1016/j.jnucmat.2016.12.015.
[37] Y. Ding, Z. Cao, Q. Zhong, G. Ran, Hydrogen modified dislocation loop types and shapes in irradiated iron, Scr. Mater. 255 (2025) 116376, https://doi.org/10.1016/j.scriptamat.2024.116376.
[38] Y.-R. Lin, W.-Y. Chen, M. Li, J. Henry, S.J. Zinkle, Dynamic observation of dual-beam irradiated Fe and Fe-10Cr alloys at 435 °C, Acta Mater. 209 (2021) 116793, https://doi.org/10.1016/j.actamat.2021.116793.
[39] A. Bhattacharya, J. Henry, B. Décamps, S.J. Zinkle, E. Meslin, Helium causing disappearance of a/2<111> dislocation loops in binary Fe-Cr ferritic alloys, J. Nucl. Mater. 556 (2021) 153213, https://doi.org/10.1016/j.jnucmat.2021.153213.
[40] Y. Zhang, Z. Xiao, X.-M. Bai, Effect of Cr concentration on 1/2<111> to <100> dislocation loop transformation in Fe-Cr alloys, J. Nucl. Mater. 543 (2021) 152592, https://doi.org/10.1016/j.jnucmat.2020.152592.
[41] S. Plimpton, Fast parallel algorithms for short-range molecular dynamics, J. Comput. Phys. 117 (1995) 1–19, https://doi.org/10.1006/jcph.1995.1039.

[42] D. Terentyev, L. Malerba, P. Klaver, P. Olsson, Formation of stable sessile interstitial complexes in reactions between glissile dislocation loops in bcc Fe, J. Nucl. Mater. 382 (2008) 126–133, https://doi.org/10.1016/j.jnucmat.2008.08.031.
[43] G. Henkelman, B.P. Uberuaga, H. Jónsson, A climbing image nudged elastic band method for finding saddle points and minimum energy paths, J. Chem. Phys. 113 (2000) 9901–9904, https://doi.org/10.1063/1.1329672.
[44] A. Stukowski, K. Albe, Extracting dislocations and non-dislocation crystal defects from atomistic simulation data, Model. Simulat. Mater. Sci. Eng. 18 (2010) 085001, https://doi.org/10.1088/0965-0393/18/8/085001.
[45] G.J. Ackland, M.I. Mendelev, D.J. Srolovitz, S. Han, A.V. Barashev, Development of an interatomic potential for phosphorus impurities in α-iron, J. Phys. Condens. Matter 16 (2004) S2629, https://doi.org/10.1088/0953-8984/16/27/003.
[46] L. Malerba, M.C. Marinica, N. Anento, C. Björkas, H. Nguyen, C. Domain, F. Djurabekova, P. Olsson, K. Nordlund, A. Serra, D. Terentyev, F. Willaime, C.S. Becquart, Comparison of empirical interatomic potentials for iron applied to radiation damage studies, J. Nucl. Mater. 406 (2010) 19–38, https://doi.org/10.1016/j.jnucmat.2010.05.017.
[47] G.J. Ackland, D.J. Bacon, A.F. Calder, T. Harry, Computer simulation of point defect properties in dilute Fe-Cu alloy using a many-body interatomic potential, Philos. Mag. A 75 (1997) 713–732, https://doi.org/10.1080/01418619708207198.
[48] M.I. Mendelev, S. Han, D.J. Srolovitz, G.J. Ackland, D.Y. Sun, M. Asta, Development of new interatomic potentials appropriate for crystalline and liquid iron, Philos. Mag. 83 (2003) 3977–3994, https://doi.org/10.1080/14786430310001613264.
[49] A. Stukowski, Visualization and analysis of atomistic simulation data with OVITO–the Open Visualization Tool, Model. Simulat. Mater. Sci. Eng. 18 (2010) 015012, https://doi.org/10.1088/0965-0393/18/1/015012.
[50] Y.N. Osetsky, A. Serra, V. Priego, Interactions between mobile dislocation loops in Cu and α-Fe, J. Nucl. Mater. 276 (2000) 202–212, https://doi.org/10.1016/S0022-3115(99)00179-8.
[51] F. Willaime, C.C. Fu, M.C. Marinica, J. Dalla Torre, Stability and mobility of self-interstitials and small interstitial clusters in α-iron: ab initio and empirical potential calculations, Nucl. Instrum. Methods Phys. Res., Sect. B 228 (2005) 92–99, https://doi.org/10.1016/j.nimb.2004.10.028.
[52] R. Alexander, M.C. Marinica, L. Proville, F. Willaime, K. Arakawa, M.R. Gilbert, S.L. Dudarev, Ab initio scaling laws for the formation energy of nanosized interstitial defect clusters in iron, tungsten, and vanadium, Phys. Rev. B 94 (2016) 024103, https://doi.org/10.1103/PhysRevB.94.024103.
[53] F.A. Garner, M.B. Toloczko, B.H. Sencer, Comparison of swelling and irradiation creep behavior of fcc-austenitic and bcc-ferritic/martensitic alloys at high neutron exposure, J. Nucl. Mater. 276 (2000) 123–142, https://doi.org/10.1016/S0022-3115(99)00225-1.
[54] F. Hofmann, D. Nguyen-Manh, M.R. Gilbert, C.E. Beck, J.K. Eliason, A.A. Maznev, W. Liu, D.E.J. Armstrong, K.A. Nelson, S.L. Dudarev, Lattice swelling and modulus change in a helium-implanted tungsten alloy: X-ray micro-diffraction, surface acoustic wave measurements, and multiscale modelling, Acta Mater. 89 (2015) 352–363, https://doi.org/10.1016/j.actamat.2015.01.055.
[55] J.P. Barrett, The coefficient of determination—some limitations, Am. Statistician 28 (1974) 19–20, https://doi.org/10.1080/00031305.1974.10479056.
[56] Y. Mu, X. Liu, L. Wang, A Pearson's correlation coefficient based decision tree and its parallel implementation, Inf. Sci. 435 (2018) 40–58, https://doi.org/10.1016/j.ins.2017.12.059.
[57] D. Terentyev, F. Bergner, Y. Osetsky, Cr segregation on dislocation loops enhances hardening in ferritic Fe-Cr alloys, Acta Mater. 61 (2013) 1444–1453, https://doi.org/10.1016/j.actamat.2012.11.021.
[58] D. Terentyev, A. Bakaev, Radiation-induced strengthening and absorption of dislocation loops in ferritic Fe-Cr alloys: the role of Cr segregation, J. Phys. Condens. Matter 25 (2013) 265702, https://doi.org/10.1088/0953-8984/25/26/265702.